e-ISSN: 2687-6698

Research Article

Turkish Journal of

Analytical Chemistry

TurkJAC

https://dergipark.org.tr/tr/pub/turkjac

Synthesis of high beta-phase content granules from recycled PVDF material: Effect of process parameters and ceramic fillers

Raşit Sezer[1,2] *, **Ahmet Buğra Başer**[3]

[1] Karadeniz Technical University, Department of Metallurgical and Materials Engineering, 61080, Trabzon, Türkiye
[2] Strolabs R&D and Engineering Services, Trabzon Teknokent, 61080, Trabzon, Türkiye
[3] Boğaziçi University, Technology Transfer Office, 34342, İstanbul, Türkiye

Abstract

Polyvinylidene fluoride (PVDF) is a high-performance semi-crystalline polymer widely employed in biomedical, electronic, and energy devices owing to its excellent piezoelectricity, thermal stability, and mechanical strength. These properties are strongly governed by its polymorphic phase composition, particularly the electroactive β-phase. In this study, a sustainable upcycling approach is presented for the fabrication of β-phase–enriched PVDF granules by recycling post-used PVDF rods. The recycled material was dissolved in N,N-dimethylformamide (DMF) and subsequently precipitated into deionized water under controlled thermal conditions. The influence of precipitation temperature, polymer concentration, and ceramic filler type on β-phase formation was systematically investigated. Fourier Transform Infrared (FTIR) spectroscopy was employed to quantify the relative contents of the electroactive β- and nonpolar α-phases. The results reveal that lower precipitation temperatures (0 °C) and higher PVDF concentrations (1:10 PVDF/DMF ratio) markedly promote β-phase crystallization, with β/α ratios exceeding 0.9. Incorporation of nickel ferrite ($NiFe_2O_4$) further enhanced β-phase formation—approaching complete β-phase dominance ($\beta/\alpha \approx 1.0$) at 60 wt% loading and 0 °C—while strontium titanate ($SrTiO_3$) exerted a suppressive effect. The proposed recycling-based synthesis route not only contributes to polymer waste valorization but also offers a scalable pathway toward functional electroactive materials for piezoelectric and energy-harvesting applications.

Keywords: Polyvinylidene fluoride, FTIR, recycling, upcycling

1. Introduction

Polyvinylidene fluoride (PVDF) is a high-performance semi-crystalline polymer extensively used in biomedical, electronic, and energy-harvesting applications due to its outstanding piezoelectricity, thermal stability, and mechanical robustness [1,2]. The multifunctional behavior of PVDF arises from its ability to crystallize into several polymorphic phases—primarily α, β, and γ—each exhibiting distinct molecular conformations and electroactive characteristics (Fig. 1). The nonpolar α-phase adopts an alternating trans–gauche (TGTG′) conformation that results in antiparallel dipole alignment, whereas the β-phase exhibits an all-trans (TTTT) configuration in which dipoles are oriented in the same direction, generating strong net polarization. The γ-phase presents an intermediate TTTGTTTG′ structure with partial dipole alignment and moderate polarity [3–5].

Among these polymorphs, the β-phase is particularly attractive due to its superior electroactive properties—namely, piezoelectricity, pyroelectricity, and ferroelectricity—which make β-phase-enriched PVDF a key material for sensors, actuators, and flexible energy-harvesting systems [6–12]. Consequently, substantial research efforts have been devoted to enhancing β-phase formation through mechanical stretching, electrical poling, solvent casting, and the incorporation of polar ceramic fillers [13,14]. Electrospinning techniques have further advanced β-phase crystallization by inducing molecular chain alignment under high electric fields,

Citation: R. Sezer, A.B. Başer, Synthesis of high beta-phase content granules from recycled PVDF material: Effect of process parameters and ceramic fillers, Turk J Anal Chem, 8(1), 2026, 20–28.

***Author of correspondence:** rasitsezer@gmail.com, rsezer@ktu.edu.tr
Tel: +90 (462) 377 36 32 **Fax:** +90 (462) 325 74 05

Received: August 08, 2025 **Accepted:** November 17, 2025
https://doi.org/10.51435/turkjac.1760136

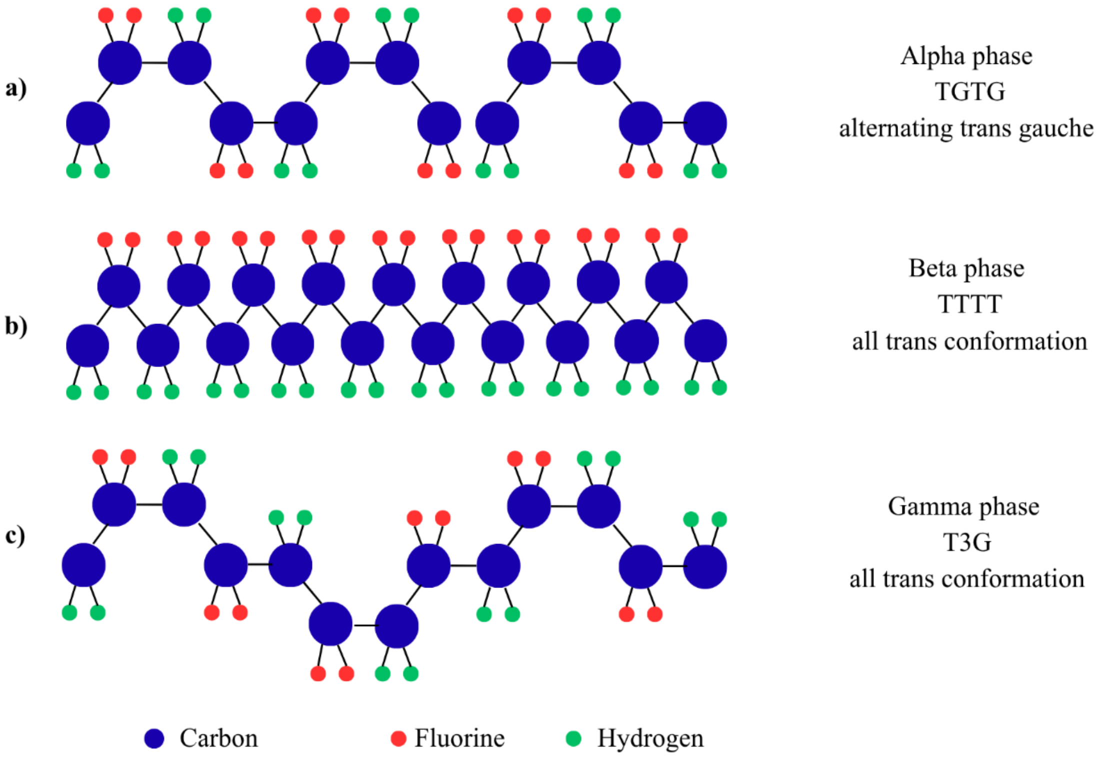

Figure 1. Chain conformations of different PVDF phases; **a)** α phase (TGTG), **b)** β phase (TTTT), **c)** γ phase (T3G)

while solvent systems such as N,N-dimethylformamide (DMF) have proven effective in stabilizing the polar crystalline structure [15–18].

The crystalline phase composition of PVDF can be effectively identified through Fourier Transform Infrared (FTIR) spectroscopy, which detects the characteristic molecular vibrations associated with different chain conformations. The interpretation of FTIR peaks is based on how the PVDF molecular chains fold and how their atomic vibrations respond to these conformations. When the chains adopt a zigzag trans–gauche–trans–gauche′ (TGTG′) configuration, corresponding to the non-polar α-phase, the $-CF_2-$ groups bend and twist in opposing directions, causing the individual dipoles to cancel each other. In contrast, when all bonds align in an all-trans (TTTT) configuration, characteristic of the electroactive β-phase, every $-CF_2-$ dipole points in the same direction, reinforcing the overall dipole moment. Therefore, by measuring the relative intensities of these vibration bands, the dominant crystalline phase of PVDF can be determined with high reliability [19,20].

In this study, we propose a sustainable method to fabricate β-phase-rich PVDF granules by recycling used PVDF rods. The process involves dissolving the material in DMF and precipitating it into deionized water at controlled temperatures. This upcycling approach not only contributes to waste valorization but also enables the development of functional materials for piezoelectric applications.

2. Materials and method

2.1. Materials and precursor preparation

Commercial polyvinylidene fluoride (PVDF, Simona) rods with a diameter of 30 mm were used as the polymer source. The rods were mechanically machined using a lathe, to obtain fine polymer shavings, which facilitated dissolution in the solvent medium. All solvents and reagents were of analytical grade and used without further purification.

2.2. Preparation of PVDF–DMF solutions and precipitation process

The PVDF shavings were dissolved in N,N-dimethylformamide (DMF, Merck) at 50 °C, under continuous magnetic stirring at 400 rpm, until a homogeneous solution was obtained. To examine the effect of polymer concentration on crystalline phase formation, three different PVDF:DMF weight ratios were used: 1:10, 1:25, and 1:50.

From each solution, 10 mL of PVDF–DMF was drawn into a glass syringe and injected dropwise into 1000 mL of deionized water maintained at three controlled precipitation temperatures of 0 °C, 25 °C, and 50 °C, respectively Magnetic stirring (300 rpm) was applied throughout the process to prevent agglomeration and ensure uniform granule formation. This solvent–nonsolvent exchange method was adapted from the procedure reported by Meng et al. [21], enabling rapid phase transformation during polymer solidification.

2.3. Incorporation of ceramic fillers

To evaluate the effect of ceramic additives on phase formation, the same precipitation process was repeated using PVDF–DMF solutions modified with ceramic fillers. Two types of ceramics were studied - Nickel ferrite ($NiFe_2O_4$) and Strontium titanate ($SrTiO_3$). Each filler was added to the PVDF–DMF solution at 20%, 40%, and 60% by weight relative to the PVDF content. The additives were manually dispersed before the injection step to ensure even distribution within the polymer matrix.

Strontium titanate ($SrTiO_3$) was synthesized by the solid-state reaction of stoichiometric amounts (Equation 1) of strontium carbonate ($SrCO_3$) and titanium dioxide (TiO_2), following the procedure reported by Rocha-Rangel et al. [22]. The mixed powders were thoroughly ground and calcined in air at 1000 °C for 2 hours to form the perovskite phase according to the following reaction [22]:

$$SrCO_3 + TiO_2 \rightarrow SrTiO_3 + CO_2 \tag{1}$$

Nickel ferrite ($NiFe_2O_4$) was prepared using a solution combustion synthesis route, following the procedure and reaction pathway reported by Jain et al [23]. Stoichiometric amounts (Equation 2) [23] of nickel nitrate and iron nitrate salts were dissolved in distilled water along with citric acid (used as fuel and a chelating agent). After adjusting the pH to neutral using ammonia solution (25% NH_4OH), the solution was heated until gelation occurred, followed by spontaneous combustion. The resulting ash was then calcined at 1000 °C for 2 hours to obtain phase-pure $NiFe_2O_4$ nanoparticles.

$$\begin{aligned} &Ni(NO_3)_2.6H_2O + 2\,Fe(NO_3)_3.9H_2O + 2.2\,C_6H_8O_7.H_2O \\ &\quad \rightarrow NiFe_2O_4 + 35.1\,H_2O + 4\,N_2 + 13.3\,CO_2 \end{aligned} \tag{2}$$

The experimental parameters applied during the fabrication of pure PVDF polymers and ceramic-filled PVDF composites are summarized in Table 1.

Table 1. Summary of experimental parameters for PVDF and PVDF–ceramic composites

PVDF:DMF ratio (w/v)	Precipitation Temperature (°C)	$NiFe_2O_4$ ratio (%w)	$SrTiO_3$ ratio (%w)
1:10, 1:25, 1:50	0, 25, 50	0, 20, 40, 60	0, 20, 40, 60

2.4. Characterization

The crystalline phase composition of PVDF and its composites was characterized using Fourier Transform Infrared (FTIR) Spectroscopy, which is a well-established technique for identifying the polymorphic forms of PVDF based on their unique vibrational signatures. The primary objective of this analysis was to quantify the relative contents of the electroactive β-phase, the non-polar α-phase, thereby assessing how different processing parameters affect phase formation and transformation.

Although a variety of peak assignments for different PVDF phases exist in the literature (Table 2) due to variations in sample processing and instrumentation, this study adopted two widely accepted characteristic peaks for consistent evaluation:

763 cm^{-1}: indicative of the α-phase, associated with CF_2 bending and skeletal vibrations

840 cm^{-1}: assigned to the β-phase, linked to CH_2 rocking and CF_2 stretching in the all-trans (TTTT) conformation

Table 2. FTIR wave frequencies of different PVDF phases

PVDF Phase	Wavenumber frequency (cm^{-1})
α-phase	613[16], 763[16,24], 796[16], 974[16], 1402[16]
β-phase	510[25], 840[26,27], 1279[25]
γ-phase	431[25], 833[25], 1234[28], 1233[29]
δ-phase	510-530[5]

These peaks were chosen based on their high spectral specificity and minimal overlapping with adjacent bands, allowing for accurate phase discrimination and quantification.

FTIR spectra were recorded in transmittance mode, and the transmittance (T) values were subsequently converted to absorbance (A) using the logarithmic relation:

$$A = 2 - 2\,\log(T) \tag{3}$$

To determine the relative β-phase fraction (fβ) with respect to the α-phase, the following (Equation 4) was employed:

$$f\beta = \frac{A\beta}{1.26 * A\alpha + A\beta} \tag{4}$$

where; Aα and Aβ are the absorbance values at 763 cm^{-1} and 840 cm^{-1}, respectively, 1.26 is a calibration factor accounting for differences in absorption coefficients.

A total of 63 samples were analyzed using this method to provide a systematic comparison of how solvent (DMF) concentration, precipitation temperature, and ceramic filler composition influence PVDF's crystalline behavior.

3. Results and discussion

The development of the electroactive β-phase in PVDF strongly depends on thermal and compositional parameters. In this study, the β/α phase ratio was employed as a quantitative indicator of electroactivity.

The combined effects of precipitation temperature, polymer concentration, and ceramic filler type were systematically analyzed.

3.1. Beta phase fraction in the pure PVDF granules

3.1.1. *Effect of precipitation temperature*

One of the most dominant factors influencing the β/α phase ratio was the temperature of the deionized water bath during the PVDF precipitation process. As shown by Fig. 2, lower precipitation temperatures strongly favored the formation of the β-phase.

From the FTIR transmittance data, the ratio of beta and alpha (β/α) calculated via Equation 4. The temperature of the deionized water during PVDF precipitation had the most significant impact on the β-phase formation. It was observed that low-temperature conditions (0 °C) consistently yielded the highest β/α phase ratios, often exceeding 0.90. This is attributed to rapid solvent exchange and fast chain solidification, which favor the all-trans (TTTT) conformation required for β-phase nucleation. The abrupt cooling limits the polymer chains' ability to reorganize into the more thermodynamically stable β-phase.

At 25 °C, the formation of the β-phase was moderate, whereas at 50 °C the FTIR spectra revealed a noticeable increase in α-phase peaks. This behavior can be attributed to the enhanced molecular mobility at elevated temperatures, which enables PVDF chains to relax into the thermodynamically more stable zigzag trans–gauche–trans–gauche′ (TGTG′) conformation characteristic of the α-phase.

When examining the XRD patterns (Fig. 2d), it was observed that for samples with a constant PVDF/DMF ratio of 1:10, the PVDF granules precipitated at 0 °C exhibited a broad diffraction peak at 2θ = 20.08°, which corresponds to the overlapping characteristic reflections of the β-phase (110) and (200) planes [30,31]. In addition, a weaker diffraction peak appearing at 36° can be attributed to the (201) plane of the β-phase [30]. A minor peak around 40° was also detected, corresponding to the γ- and α-phase reflections [31]. These results indicate that the PVDF granules obtained at 0 °C predominantly exhibit the electroactive β-phase structure.

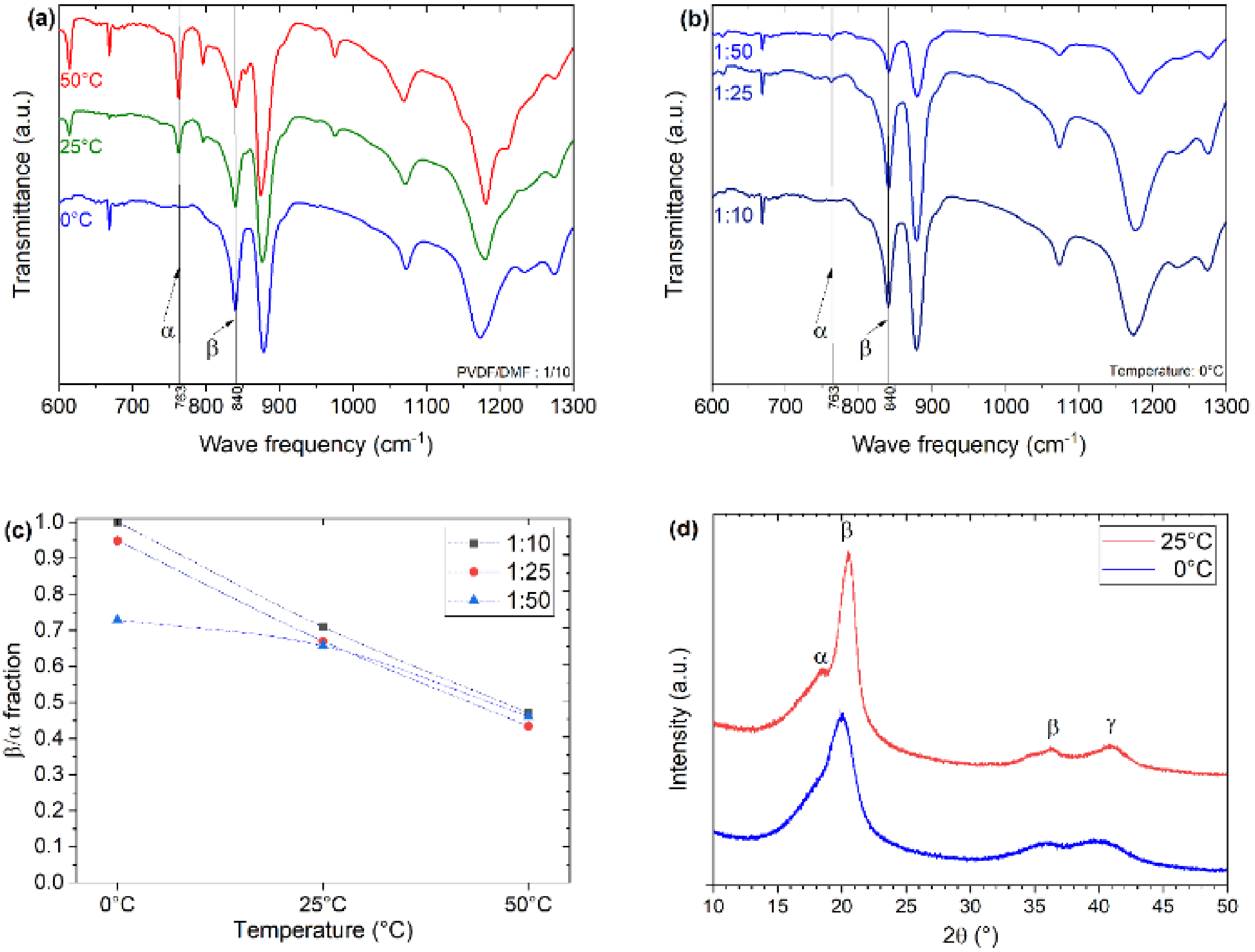

Figure 2. FTIR analysis of PVDF granules precipitated (**a**) at different temperatures with PVDF/DMF:1/10, (**b**) from the solutions with different concentration at 0°C, (**c**) calculated β/α fractions and (**d**) XRD patterns of granules precipitated at 0 and 25°C PVDF/DMF:1/10

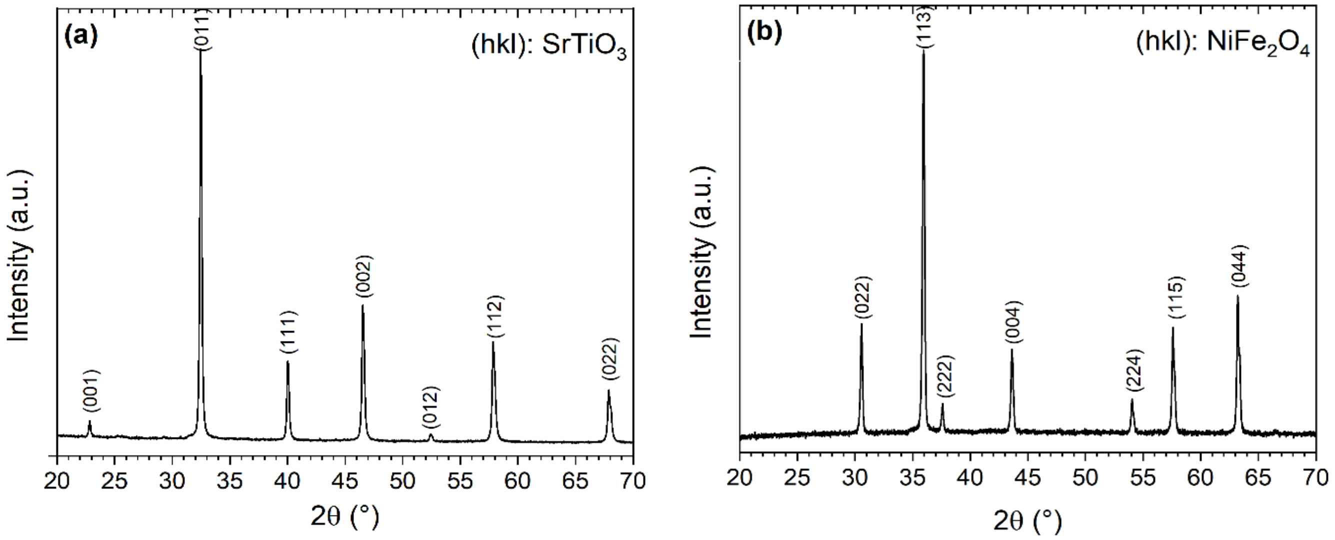

Figure 3. XRD patterns of ceramic filler: (**a**) $SrTiO_3$ and (**b**) $NiFe_2O_4$

However, when the precipitation temperature was increased to 25 °C, a distinct diffraction peak emerged at 18.30°, corresponding to the (020) plane of the α-phase, [30,31] confirming the increased presence of the non-polar α-phase at higher temperatures.

These results align well with the findings of Ghafari et al. [32] and Ma et al. [7], who reported enhanced β-phase content under low-temperature or quenching conditions. The present study confirms and reinforces the critical role of thermal kinetics in guiding phase development in PVDF.

3.1.2. *Effect of solvent concentration (PVDF/DMF Ratio)*

Another critical factor was the polymer concentration in the solvent. The FTIR analysis of the PVDF granules are given in Fig. 3. The β/α ratio was highest in samples prepared with a 1:10 PVDF/DMF ratio, indicating that concentrated solutions facilitate β-phase crystallization. This can be attributed to several factors: increased chain–chain interactions at higher PVDF concentrations; higher viscosity, which restricts molecular rearrangement during precipitation, a denser polymer network, which supports ordered nucleation.

In contrast, more dilute solutions (1:25 and 1:50) led to significantly lower β/α ratios, particularly at 50 °C. Dilution reduces chain–chain interactions and increases chain mobility, promoting the β-phase. These findings are consistent with Szewczyk et al. [9] and Kim et al. [14], who demonstrated that polymer density influences the phase outcome during solvent casting and electrospinning.

3.2. Effect of ceramic fillers

3.2.1. *Structural characterization of ceramic fillers*

To confirm the successful synthesis and phase purity of the ceramic fillers used in this study, X-ray diffraction (XRD) analysis was performed on both strontium titanate ($SrTiO_3$) and nickel ferrite ($NiFe_2O_4$) powders. The XRD patterns are presented in Fig. 3.

The XRD pattern of $SrTiO_3$ (Fig. 3a) shows sharp and well-defined peaks corresponding to the cubic perovskite phase (space group Pm-3m). The most intense diffraction peaks are listed in Table 3 and are indexed to the corresponding (hkl) planes according to the reference JCPDS card. These reflections are in good agreement with the standard JCPDS card No. 35-0734 [33], confirming the successful formation of a single-phase $SrTiO_3$ structure. The absence of any secondary peaks suggests that the solid-state synthesis route used—based on the calcination of stoichiometric $SrCO_3$ and TiO_2 at 1100 °C—was effective in yielding a phase-pure $SrTiO_3$ material. The sharpness and intensity of the peaks also indicate high crystallinity, which is desirable for filler uniformity in composite matrices.

The XRD pattern of $NiFe_2O_4$ (Fig. 3b) reveals distinct peaks that are characteristic of the spinel cubic structure (space group Fd-3m) of nickel ferrite. The most prominent diffraction peaks are indexed to the corresponding (hkl) planes, as summarized in Table 3, and show excellent agreement with the reference data for the spinel $NiFe_2O_4$ structure. These match well with

Table 3. XRD diffraction peaks lists of the ceramic fillers

$SrTiO_3$	**JCPDS Card**	2θ (°)	22.8	32.4	39.9	46.4	52.6	58.9	67.9
	35-0734	(hkl)	(001)	(011)	(111)	(002)	(012)	(112)	(022)
$NiFe_2O_4$	**JCPDS Card**	2θ (°)	30.3	32.4	39.9	46.4	52.6	58.9	67.9
	10-0325	(hkl)	(022)	(113)	(222)	(004)	(224)	(115)	(044)

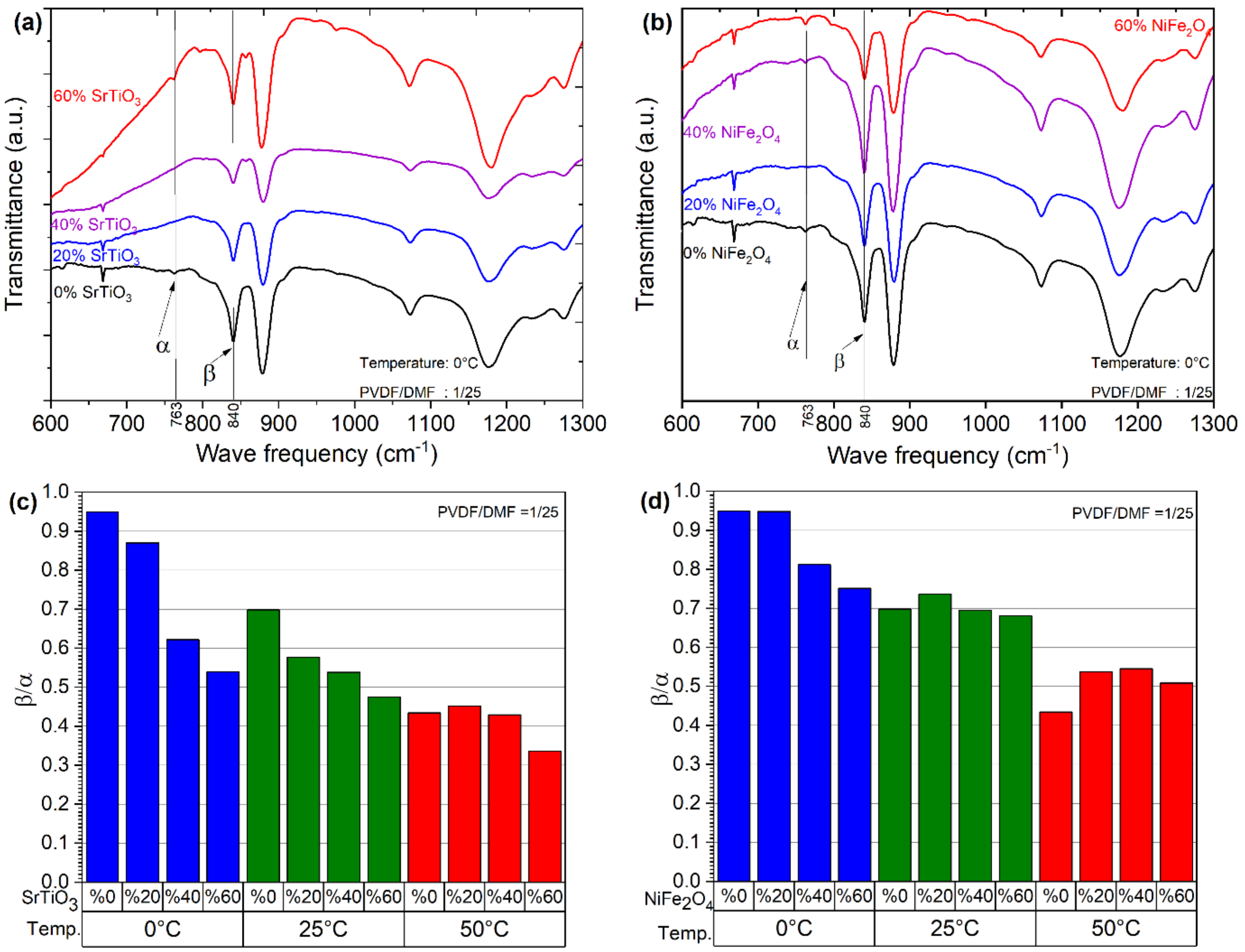

Figure 4. FTIR analysis of composite granules filled with (**a**) $SrTiO_3$ and (**b**) $NiFe_2O_4$; calculated β/α fraction of (**c**) $SrTiO_3$ and (**d**) $NiFe_2O_4$ filled granules

the standard JCPDS card No. 10-0325 [34], confirming the formation of the $NiFe_2O_4$ spinel phase.

No impurity peaks (such as unreacted NiO_x or FeO_x) were observed, suggesting that the auto-combustion synthesis method, followed by post-calcination at 1100 °C, successfully produced phase-pure nickel ferrite. The relatively broad peak widths, in comparison to $SrTiO_3$, may indicate slightly smaller crystallite sizes or lattice strain, which is consistent with the combustion-derived synthesis routes.

The confirmed phase purity and high crystallinity of both ceramic powders are crucial for their role as functional fillers in PVDF composites. While $SrTiO_3$ offers high dielectric constants, $NiFe_2O_4$ combines magnetic properties with potential nucleation behavior. The phase-pure state ensures that no unexpected interactions or side phases will interfere with the crystalline phase transformation of PVDF, which is the central focus of this study.

In this study, the effect of ceramic fillers—strontium titanate ($SrTiO_3$) and nickel ferrite ($NiFe_2O_4$)—on the formation of the electroactive β-phase in PVDF was systematically investigated under varying temperatures (0 °C, 25 °C, 50 °C) and filler concentrations (0%, 20%, 40%, 60%). FTIR spectra and corresponding β/α phase ratio bar graphs presented in Fig. 4 (a–b) and the charts below (Fig. 4 c–d) clearly demonstrate how ceramic additions modify the phase composition of PVDF.

3.2.2. *$SrTiO_3$-filled composites*

The incorporation of $SrTiO_3$ particles into PVDF/DMF solutions revealed a concentration-dependent suppression of β-phase formation at all temperatures (Fig. 3c). At 0 °C, the β/apα ratio dropped from approximately 0.94 for neat PVDF to 0.88, 0.65, and 0.51 with increasing $SrTiO_3$ contents (20%, 40%, and 60%, respectively). This trend is consistently observed at 25 °C and 50 °C, though overall β/α values are lower at higher temperatures.

This reduction in β-phase content may be attributed to the non-polar surface nature of $SrTiO_3$ nanoparticles, which possibly interferes with dipolar chain alignment of PVDF, reducing the stabilization of all-trans β-phase. Moreover, increased filler content can disturb crystallization kinetics by serving as heterogeneous

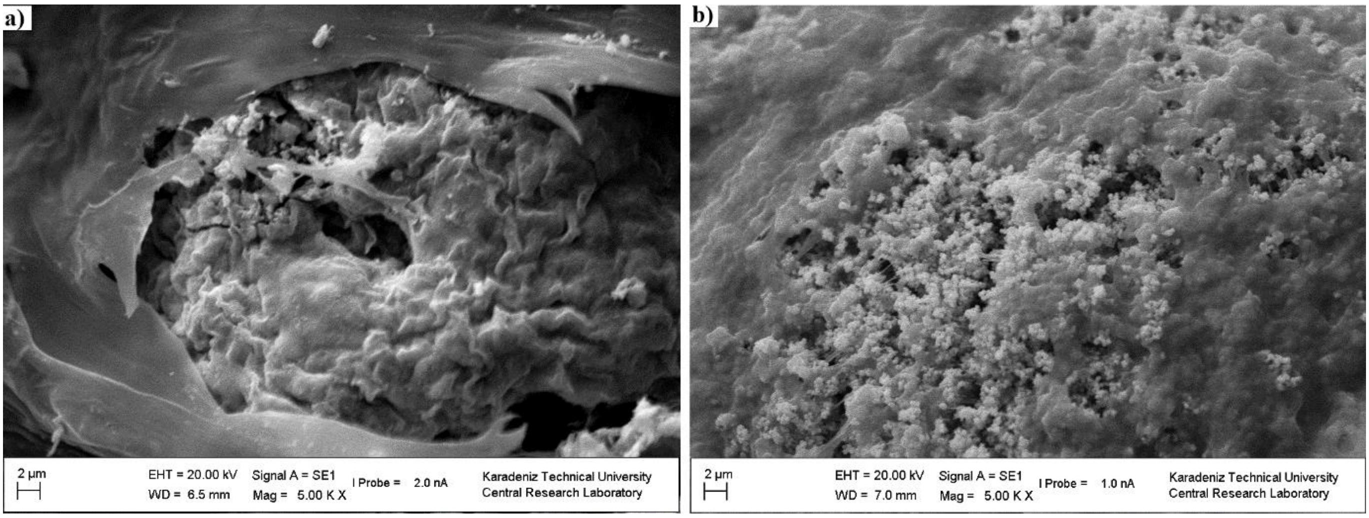

Figure 5. SEM images of a) %60 $NiFe_2O_4$ and b) %60 $SrTiO_3$ filled PVDF granules precipitated at 0°C from the solution PVDF/DMF:1/25

nucleation sites that do not preferentially promote β-phase nucleation.

The SEM micrographs clearly reveal the influence of ceramic filler type on the microstructural morphology of the PVDF granules. In Fig. 5a, $NiFe_2O_4$-filled PVDF exhibits a dense and compact morphology, indicating strong interfacial adhesion between the magnetic nanoparticles and the polymer matrix. This improved interaction is consistent with the enhanced β-phase crystallization observed in FTIR analyses. Conversely, Fig. 5b shows that $SrTiO_3$-filled PVDF granules have a more porous and loosely packed surface, with visible nanoparticle agglomerations. This morphology suggests limited polymer–filler compatibility, which can hinder dipole alignment and consequently reduce β-phase formation efficiency.

These observations align with previous literature suggesting that ceramic fillers lacking strong polar interaction with PVDF chains may hinder β-phase formation, unless surface functionalization or orientation-inducing methods (e.g., electrical poling) are applied [35].

3.2.3. $NiFe_2O_4$-filled composites

In contrast to $SrTiO_3$, $NiFe_2O_4$ additions significantly enhanced β-phase formation, especially at low temperatures (Fig. 4b). At 0°C, the β/α ratio increased with filler content, peaking at approximately 1.0 for 60% $NiFe_2O_4$ loading. This enhancement is sustained, though gradually decreasing, at 25 °C and 50 °C, suggesting a temperature-filler interaction effect.

The magnetic nature and high surface energy of $NiFe_2O_4$ nanoparticles are likely to facilitate better interaction with PVDF chains, promoting the trans-conformation alignment necessary for β-phase crystallization. Unlike ionic fillers, $NiFe_2O_4$ does not ionize in solution, but its interface with the polymer matrix can still influence crystallization behavior via physical interactions.

These findings are in agreement with prior studies reporting that magnetic ferrite fillers promote electroactive β-phase crystallization due to their ability to align dipoles during processing [6,8]. Moreover, similar improvements have been observed with Fe_3O_4 and $CoFe_2O_4$ fillers in PVDF matrices [7].

In both $SrTiO_3$ and $NiFe_2O_4$ series, increasing the processing temperature led to a notable decrease in β/α ratios, regardless of filler content. This outcome is likely due to the enhanced molecular mobility at higher temperatures, allowing PVDF chains to revert to the more thermodynamically stable but electroinactive α-phase conformation. Low temperatures, especially 0 °C, effectively 'freeze' the polymer chains in the polar β-phase during precipitation from DMF.

These findings corroborate well with the reports of Kim et al. [14] and Esmaeili et al. [1], who also observed higher β-phase formation in PVDF when processed under rapid quenching or low-temperature conditions.

4. Conclusion

This work presents a sustainable and scalable approach for fabricating β-phase–enriched PVDF granules through the upcycling of post-used PVDF rods. The controlled precipitation of PVDF from DMF into deionized water enabled systematic tuning of crystalline phase composition. The findings demonstrate that lower precipitation temperatures (0 °C) and higher PVDF concentrations (1:10 PVDF/DMF ratio) significantly promote β-phase formation by restricting molecular mobility during rapid solvent exchange.

The incorporation of ceramic fillers revealed distinct effects on phase transformation. Nickel ferrite ($NiFe_2O_4$) markedly enhanced β-phase crystallization, achieving nearly complete β-phase dominance ($\beta/\alpha \approx 1.0$) at 60 wt%

loading and 0 °C, whereas strontium titanate ($SrTiO_3$) exhibited a suppressive influence due to its nonpolar surface chemistry. These results confirm that both thermokinetic parameters and interfacial filler–polymer interactions critically dictate PVDF's crystalline behavior.

Overall, the proposed recycling-based synthesis route contributes to polymer waste valorization and offers a viable pathway toward the development of high-performance electroactive materials for sensors, actuators, and energy-harvesting devices. Future studies should further explore granule morphology optimization, long-term stability, and device-level piezoelectric characterization to fully realize the potential of recycled PVDF-based materials.

References

[1] E. Esmaeili, M. Soleimani, M.A. Ghiass, S. Hatamie, S. Vakilian, M.S. Zomorrod, N. Sadeghzadeh, M. Vossoughi, S. Hosseinzadeh, Magnetoelectric nanocomposite scaffold for high yield differentiation of mesenchymal stem cells to neural-like cells, J Cell Physiol, 234, 2018, 13617–13628.

[2] S. Mohammadpourfazeli, S. Arash, A. Ansari, S. Yang, K. Mallick, R. Bagherzadeh, Future prospects and recent developments of polyvinylidene fluoride (PVDF) piezoelectric polymer; fabrication methods, structure, and electro-mechanical properties, RSC Adv, 13, 2023, 370-387.

[3] F. Ali, I. Parvez, M.I. Albakri, Enhancing the electroactive β-phase of PVDF filaments via feedstock processing, Smart Mater Struct, 34, 2025, 035012.

[4] S. Swain, R. Lenka, T. Rautray, Synthetic strategy for the production of electrically polarized polyvinylidene fluoride-trifluoroethylene—co-polymer osseo-functionalized with hydroxyapatite scaffold, J Biomed Mater Res A, 112, 2024, 1675-1687.

[5] M. Krutko, H.M. Poling, A. Bryan, M. Sharma, A. Singh, H.A. Reza, K.A. Wikenheiser-Brokamp, T. Takebe, M.A. Helmrath, G.M. Harris, L. Esfandiari, Enhanced piezoelectric performance of PVDF-TRFE nanofibers through annealing for tissue engineering applications, bioRxiv, 2024.

[6] S. Garain, S. Jana, T.K. Sinha, D. Mandal, Design of in situ poled Ce3+-doped electrospun PVDF/graphene composite nanofibers for fabrication of nanopressure sensor and ultrasensitive acoustic nanogenerator, ACS Appl Mater Interfaces, 8, 2016, 4532-4540.

[7] S. Ma, Q. Sun, Y. Su, R. Chen, L. Wang, Experimental investigation of piezoelectricity of near field electrospun PVDF nanofibers, Telkomnika, 14, 2016, 145-151.

[8] M. Sahu, S. Hajra, K. Lee, P.L. Deepti, K. Mistewicz, H.J. Kim, Piezoelectric nanogenerator based on lead-free flexible PVDF-barium titanate composite films for driving low power electronics, Crystals, 11, 2021, 85.

[9] P.K. Szewczyk, A. Gradys, S.K. Kim, L. Persano, M. Marzec, A. Kryshtal, T. Busolo, A. Toncelli, D. Pisignano, A. Bernasik, S. Kar-Narayan, P. Sajkiewicz, U. Stachewicz, Enhanced piezoelectricity of electrospun polyvinylidene fluoride fibers for energy harvesting, ACS Appl Mater Interfaces, 12, 2020, 13575–13583.

[10] A. Jain, S. Minajagi, E. Dange, S.U. Bhover, Y.T. Dharanendra, Impact and acoustic emission performance of polyvinylidene fluoride sensor embedded in glass fiber-reinforced polymer composite structure, Polym Polym Compos, 29, 2020, 354-361.

[11] J. Pärssinen, H. Hammarén, R. Rahikainen, V. Sencadas, C. Ribeiro, S. Vanhatupa, S. Miettinen, S. Lanceros-Méndez, V.P. Hytönen, Enhancement of adhesion and promotion of osteogenic differentiation of human adipose stem cells by poled electroactive poly(vinylidene fluoride), J Biomed Mater Res A, 103, 2014, 919-928.

[12] L. Ruan, X. Yao, Y. Chang, L. Zhou, G. Qin, X. Zhang, Properties and applications of the β phase poly(vinylidene fluoride), Polymers, 10, 2018, 228.

[13] J.S. Andrew, D.R. Clarke, Enhanced ferroelectric phase content of polyvinylidene difluoride fibers with the addition of magnetic nanoparticles, Langmuir, 24, 2008, 8435–8438.

[14] G.H. Kim, S.M. Hong, Y. Seo, Piezoelectric properties of poly(vinylidene fluoride) and carbon nanotube blends: β-phase development, Phys Chem Chem Phys, 11, 2009, 10506-10512.

[15] C. Hwang, W. Song, G. Song, Y. Wu, S. Lee, H.B. Son, J. Kim, N. Liu, S. Park, H. Song, A three-dimensional nano-web scaffold of ferroelectric beta-PVDF fibers for lithium metal plating and stripping, ACS Appl Mater Interfaces, 12, 2020, 29235–29241.

[16] T. Nguyen, P.N. Vu, H.T. Trinh, Enhancement of the crystalline phase in poly(vinylidene fluoride) by using the electrospinning technique and graphene oxide composition, Sci Tech Dev J, 26, 2023, 2741-2747.

[17] S. Kaniapan, A. Prathuru, N.H. Faisal, Spin-coated synthesis of polyvinylidene fluoride-barium titanate nanocomposite piezoelectric flexible thin films, Proc SPIE 13205, Advanced Materials, Biomaterials, and Manufacturing Technologies for Security and Defence II, 2024, United Kingdom, 1320509.

[18] N. Govinna, I. Sadeghi, A. Asatekin, P. Cebe, Thermal properties and structure of electrospun blends of PVDF with a fluorinated copolymer, J Polym Sci Part B Polym Phys, 57, 2019, 312–322.

[19] M. Sharma, J.K. Quamara, A. Gaur, Behaviour of multiphase PVDF in (1−x)PVDF/(x)BaTiO3 nanocomposite films: structural, optical, dielectric and ferroelectric properties, J Mater Sci Mater Electron, 29, 2018, 10875–10884.

[20] S. Dash, R.N.P. Choudhary, M.N. Goswami, Enhanced dielectric and ferroelectric properties of PVDF-BiFeO3 composites in 0–3 connectivity, J Alloys Compd, 715, 2017, 29-36.

[21] X. Meng, Q. Li, Z. Hu, M. Guo, Microfluidic fabrication of β-phase enriched poly(vinylidene fluoride) microfibers toward flexible piezoelectric sensor, J Polym Sci, 60, 2022, 1718-1726.

[22] E. Rocha-Rangel, J. López-Hernández, J.A. Rodríguez-García, E.N. Armendáriz-Mireles, C.A. Calles-Arriaga, W.J. Pech-Rodríguez, J.A. Castillo-Robles, Dielectric properties of strontium titanate synthesized by means of solid state reactions activated mechanically, Materia-Brazil, 22, 2017, e11818.

[23] A. Jain, K. Kandwal, R. Kumar, S. Sharma, R. Dhiman, H. Sharma, K.S. Naidu, S. Gupta, A. Kumar, R. Singh, Synergistic enhancement of super capacitive performance through sol-gel auto-combustion synthesis of nickel ferrite nano-particles and reduced graphene oxide hybrid nano-composite electrode, J Inorg Organomet Polym, 2025.

[24] A.S. Zahari, M. Hafiz, I.I. Misnon, Influence of molecular weight on the morphology and structure of electrospun polyvinylidene fluoride (PVDF), Mater Sci Forum, 1025, 2021, 293–298.

[25] S.M. Seraji, Q. Guo, Nanophase morphology and crystallization in poly(vinylidene fluoride)/polydimethylsiloxane-block-poly(methylmethacrylate)-block-polystyrene blends, Polym Int, 68, 2019, 1064–1073.

[26] Y. Ahn, J. Lim, S.M. Hong, J. Lee, J. Ha, H.J. Choi, Y. Seo, Enhanced piezoelectric properties of electrospun poly(vinylidene fluoride)/multiwalled carbon nanotube composites due to high β-phase formation in poly(vinylidene fluoride), J Phys Chem C, 117, 2013, 11791–1179.

[27] R.L. Hadimani, D.V. Bayramol, N. Sion, T. Shah, L. Qian, S. Shi, E. Siores, Continuous production of piezoelectric PVDF fibre for e-textile applications, Smart Mater Struct, 22, 2013, 075017.

[28] S. Satapathy, S. Pawar, P.K. Gupta, K.B.R. Varma, Effect of annealing on phase transition in poly(vinylidene fluoride) films prepared using polar solvent, Bull Mater Sci, 34, 2011, 727–733.

[29] I.O. Pariy, A. Ivanova, V.V. Shvartsman, D.C. Lupascu, G.B. Sukhorukov, T. Ludwig, A. Bartasyte, S. Mathur, M.A. Surmeneva, R.A. Surmenev, Piezoelectric response in hybrid micropillar arrays of poly(vinylidene fluoride) and reduced graphene oxide, Polymers, 11, 2019, 1065.

[30] S. Janakiraman, A. Surendran, S. Ghosh, S. Anandhan, A. Venimadhav, Electroactive poly(vinylidene fluoride) fluoride separator for sodium ion battery with high coulombic efficiency, Solid State Ionics, 292, 2016, 130-135.

[31] Y. Zhao, W. Yang, Y. Zhou, Y. Chen, X. Cao, Y. Yang, J. Xu, Y. Jiang, Effect of crystalline phase on the dielectric and energy storage properties of poly(vinylidene fluoride), J Mater Sci Mater Electron, 27, 2016, 7280–7286.

[32] E. Ghafari, X. Jiang, N. Lu, Surface morphology and beta-phase formation of single polyvinylidene fluoride (PVDF) composite nanofibers, Adv Compos Hybrid Mater, 1, 2018, 332–340.

[33] M.V. Le, N.Q.D. Vo, Q.C. Le, V.A. Tran, T.Q.P. Phan, C.W. Huang, V.H. Nguyen, Manipulating the structure and characterization of Sr1−xLaxTiO3 nanocubes toward the photodegradation of 2-naphthol under artificial solar light, Catalysts, 11, 2021, 564.

[34] T.M. Naidu, P.V. Lakshmi Narayana, Synthesis and characterization of Fe-TiO2 and NiFe2O4 nanoparticles and its thermal properties, J Nanosci Tech, 5, 2019, 769-772.

[35] H. Abdolmaleki, S. Agarwala, PVDF-BaTiO3 nanocomposite inkjet inks with enhanced β-phase crystallinity for printed electronics, Polymers, 12, 2020, 2430.